Available online at www.sciencedirect.com
ScienceDirect
Journal of the European Ceramic Society 31 (2011) 159–166
www.elsevier.com/locate/jeurceramsoc

High-temperature thermal stability of Ti_2AlN and Ti_4AlN_3: A comparative diffraction study

I.M. Low [a,*], W.K. Pang [a], S.J. Kennedy [b], R.I. Smith [c]

[a] *Centre for Materials Research, Department of Imaging and Applied Physics, Curtin University of Technology, GPO Box U 1987, Perth, WA, Australia*
[b] *The Bragg Institute, ANSTO, Locked Bag 2001, Kirrawee DC, NSW 2232, Australia*
[c] *ISIS Facility, Science and Technology Facilities Council, Rutherford Appleton Laboratory, Harwell Science and Innovation Campus, Didcot, Oxfordshire OX11 0QX, UK*

Received 2 May 2010; received in revised form 4 September 2010; accepted 14 September 2010

Abstract

The susceptibility of Ti_2AlN and Ti_4AlN_3 to high-temperature thermal dissociation in a dynamic environment of high-vacuum has been investigated using *in situ* neutron diffraction. Under high vacuum, these ternary nitrides decomposed above 1400 °C through the sublimation of Al, and possibly Ti, to form a surface coating of TiN_x ($0.5 \leq x \leq 0.75$). The kinetics of isothermal phase decomposition were modelled using the Avrami equation and the Avrami exponents (n) of isothermal decomposition of Ti_2AlN and Ti_4AlN_3 were determined to be 0.62 and 0.18, respectively. The characteristics of thermal stability and phase transitions in Ti_2AlN and Ti_4AlN_3 are compared in terms of the rate of decomposition, phase relations and microstructures.

Keywords: Ternary nitride; Ti_2AlN; Ti_4AlN_3; Neutron diffraction; Sublimation; Thermal decomposition

1. Introduction

MAX phases are nano-layered ceramics with the general formula $M_{n+1}AX_n$ ($n = 1$–3), where M is an early transition metal, A is a group A element, and X is either carbon and/or nitrogen. These materials exhibit a unique combination of characters of both ceramics and metals.[1–5] Like ceramics, they have low density, low thermal expansion coefficient, high modulus and high strength, and good high-temperature oxidation resistance. Like metals, they are good electrical and thermal conductors, readily machinable, tolerant to damage, and resistant to thermal shock. The unique combination of these interesting properties enables these ceramics to be a promising candidate material for use in technologically important fields, especially in high temperature applications.

However, these MAX phases, and Ti_3SiC_2 in particular, are susceptible to thermal dissociation at ~1400 °C in inert environments (e.g., vacuum or argon) to form a porous surface coating of TiC.[6–11] Depth-profiling by X-ray diffraction of Ti_3SiC_2 annealed in vacuum at 1500 °C has revealed a graded phase composition with more than 90 wt% TiC on the surface and decreasing rapidly with an increase in depth.[6,7] A similar phenomenon has also been observed for Ti_3AlC_2 whereby it decomposed in vacuum to form TiC and Ti_2AlC.[10] It follows that this process of thermal dissociation to form protective coatings of binary *MX* can be expected to occur in ternary nitrides Ti_2AlN, Ti_4AlN_3 and Nb_4AlN_3.

The fundamental knowledge about the thermal stability of technologically important MAX phases is still very limited and the actual process of phase dissociation is poorly understood. This limited understanding has generated much controversy concerning the high-temperature thermochemical stability of MAX phases.[12–21] For instance, Zhang et al.[18] reported Ti_3SiC_2 to be thermally stable up to 1300 °C in nitrogen, but above this temperature drastic degradation and damage occurred due to surface decomposition. Feng et al.[19] only observed TiC on the surface of Ti_3SiC_2 annealed at 1600–2000 °C in vacuum. According to Gao et al.[20] the propensity of decomposition of Ti_3SiC_2 to TiC

* Corresponding author. Tel.: +61 9266 7544; fax: +61 8 92662377.
E-mail address: j.low@curtin.edu.au (I.M. Low).

0955-2219/$ – see front matter © 2010 Elsevier Ltd. All rights reserved.
doi:10.1016/j.jeurceramsoc.2010.09.014

was related to the vapour pressure of Si at temperatures above 1400 °C. This process of surface-initiated phase dissociation was even observed to commence as low as 1000–1200 °C in Ti_3SiC_2 thin films during vacuum annealing.[17] The large difference in observed dissociation temperatures between bulk and thin-film Ti_3SiC_2 has been attributed to the difference in diffusion length scales involved and measurement sensitivity employed in the respective studies.

In contrast, Barsoum and El-Raghy[15] observed that decomposition of Ti_3SiC_2 at 1600 °C commenced after annealing for 24 h in vacuum, but after only 4 h in an argon atmosphere. They further argued that the reduced temperature at which Ti_3SiC_2 decomposed as observed by others was due to the presence of impurity phases (e.g. Fe or V) in the starting powders which interfered with the reaction synthesis of Ti_3SiC_2, and thus destabilised it following prolonged annealing in an inert environment.[21] However, mixed results have been reported by Radakrishnan et al.[16] where Ti_3SiC_2 was shown to be stable in a tungsten-heated furnace for 10 h at 1600 °C and 1800 °C in an argon atmosphere, but dissociated to TiC_x under the same conditions when using a graphite heater. These conflicting results suggest that the thermochemical stability of MAX phases is still poorly understood although its susceptibility to thermal dissociation is strongly influenced by factors such as the purity of powders and sintered materials, temperature, sintering pressure, atmosphere, and the type of heating elements used.

Although a few studies have been conducted on the thermal stability of *312* (M_3AX_2) phases, virtually no work has been reported for the *211* (M_2AX) or *413* (M_4AX_3) phases such as Ti_2AlC, Ti_2AlN, Ta_4AlC_3 and Ti_4AlN_3. We have recently investigated the thermal stability of Ti_3SiC_2, Cr_2AlC, Ti_2AlC and Ti_3AlC_2 in vacuum at up to 1550 °C and the results indicated 211 phases to be more resistant to phase dissociation than 312 phases.[8–10] For instance, both Ti_3SiC_2 and Ti_3AlC_2 decomposed readily to TiC forming intermediate phases of Ti_5Si_3C and Ti_2AlC respectively. The apparent activation energies for the decomposition of sintered Ti_3SiC_2, Ti_3AlC_2 and Ti_2AlC were determined to be 179.3, −71.9 and 85.7 kJ mol^{-1}, respectively.[9,10]

Hitherto, virtually no work has been reported for ternary nitrides such as Ti_2AlN and Ti_4AlN_3. It also remains unknown whether these MAX phases will decompose in a similar manner to 211 and 312 ternary carbides via the sublimation of group *M* element and the de-intercalation of group *A* element as follows:

$$M_{n+1}AX_n \rightarrow (n+1)MX_{\left(\frac{n}{n+1}\right)} + A \quad (1)$$

In this paper, we describe the use of high-temperature neutron diffraction to study *in situ* the dynamic processes of phase decomposition and transitions of Ti_2AlN and Ti_4AlN_3 under high-vacuum. The kinetics of isothermal phase decomposition were modelled using the Avrami equation and the Avrami constants were evaluated. The characteristics of thermal stability and phase transitions in Ti_2AlN and Ti_4AlN_3 are compared and discussed.

2. Experimental procedure

2.1. Material synthesis

Dense hot-pressed cylindrical bar samples of Ti_2AlN and Ti_4AlN_3 with dimensions of 10 mm diameter and 20 mm height were used in this study. These samples were prepared according to the procedures previously reported by Zhou and co-workers[22] and Barsoum and co-workers,[23] respectively. The resultant samples contained ∼6.9 and ∼0.8 wt% TiN, respectively, and had ≤0.5% porosity.

2.2. In situ neutron diffraction

In situ time of flight (TOF) powder neutron diffraction was used to monitor the structural evolution of phase decomposition in Ti_2AlN at high temperature in real time. Diffraction patterns were collected using the Polaris medium resolution, high intensity powder diffractometer at the UK pulsed spallation neutron source ISIS, Rutherford Appleton Laboratory.[24] Samples were held in a basket made from thin tantalum wire and mounted in a Risø-design high temperature furnace (Risø National Laboratory, Roskilde). Fitted with a thin tantalum foil element and tantalum and vanadium heat shields, this furnace is capable of reaching 2000 °C and operates under a high dynamic (i.e., continuously pumped) vacuum (<7.5×10^{-6} Torr). Temperature monitoring and control was achieved using type W5 thermocouples, positioned ∼10 mm above the samples (so as not to be in the incident neutron beam). Collimating slits (manufactured from neutron-absorbing boron nitride) mounted on the furnace in the scattered beam direction enable diffraction patterns free from Bragg reflections off the tantalum element and heat shields to be collected in the Polaris $2\theta = 90^\circ$ detectors. A precision electronic scale (reading to five decimal places) was used to weigh the sample before it was loaded into the furnace.

For each sample, a reference diffraction pattern was collected at room temperature while the furnace was initially evacuated, then the sample was heated rapidly up to a selected temperature (e.g. 1500, 1550, 1600, 1700, and 1800 °C) where it was held constant for an extended period during which a series of diffraction patterns, each of 15 min duration, were collected. The total time spent at each elevated temperature was manually controlled, based on the level of decomposition observed in the diffraction patterns as they were collected. At the end of each high temperature measurement the furnace was cooled to room temperature, and the sample carefully removed from the furnace and weighed again in order to determine the mass of titanium and aluminium lost through evaporation.

Normalised data collected in the 2θ ∼90° detector bank over the time-of flight range (1500–19200 μs (corresponding to a *d*-spacing range of ∼0.4–4.2 Å)) were analysed using (a) the LAMP software and (b) the Fullprof software to compute the changes in the phase content of MAX phases and TiN formed during vacuum-annealing at elevated temperatures. In the former, the integrated peak intensities of lines (0 1 3) and (1 1 1) were used for calculating the relative phase content of Ti_4AlN_3 and TiN respectively. In the latter, the Rietveld method was

used to compute the phase content of Ti_2AlN and TiN during vacuum-annealing. The Rietveld method is a least-square-based refinement method which is used to obtain the best fit between the calculated and the observed diffraction patterns.[25] This method is widely used for refining crystal structural data using powder diffraction data to extract phase-specific information from materials. In the least-square procedure, a best-fitted model is obtained when the residuals (R_{wp}, R_{exp}, GOF) are minimised whereby,

$$R_{wp} = \left\{ \frac{\sum w_i[Y_i(obs) - Y_i(calc)]^2}{\sum w_i[Y_i(obs)]^2} \right\}^{1/2}$$

$$R_{exp} = \left[\frac{N - P}{\sum w_i Y_i^2(obs)} \right]^{1/2}$$

$$GOF = \left[\frac{R_{wp}}{R_{exp}} \right]^2 = \frac{\sum w_i[Y_i(obs) - Y_i(calc)]^2}{N - P}$$

Here, $I(obs)$ is the "observed" integrated intensity of Bragg reflection at the end of the refinement after distributing the contributing peaks and background to the calculated integrated intensity $I(calc)$; N is the number of observations; P is the number of adjusted parameters; $N - P$ is the number of degrees of freedom in the least squares system; GOF denotes the goodness-of-fit of the calculated pattern to the experimental.

The variation of unit cell volume as a function of temperature was determined and the coefficient of linear thermal expansion (CTE) was evaluated using the equation:

$$CTE = \frac{\Delta V}{V \Delta T} \quad (2)$$

The kinetic behaviour of the isothermal decomposition of Ti_4AlN_3 and Ti_2AlN at 1500 and 1550 °C, respectively, was modelled using the Avrami equation to describe the fraction of decomposed MAX phase (y) as a function of time (t):[26]

$$y = \exp(-kt^n) \quad (3)$$

where k and n are time-independent constants for the particular reaction.

2.3. Synchrotron radiation diffraction

Thin flat-plates of Ti_4AlN_3 and Ti_2AlN, which had been vacuum-decomposed at various temperatures were analysed on beamline 20B of the Photon Factory using the BIGDIFF diffractometer.[27] Imaging plates were used to record the patterns over the 2θ range of 2–90°. The diffractometer was operated in Debye–Scherrer mode under vacuum with wavelength of 0.7 Å and at an incident angle of 3°.

2.4. Scanning electron microscopy

The surface microstructures of the decomposed samples were examined using scanning electron microscopy. The images were acquired using SEM (Manufacturer: Zeiss, Germany; Model: EVO 40XVP) with an accelerating voltage of 15 keV. The samples were not gold or carbon-coated prior to the microstructure examination.

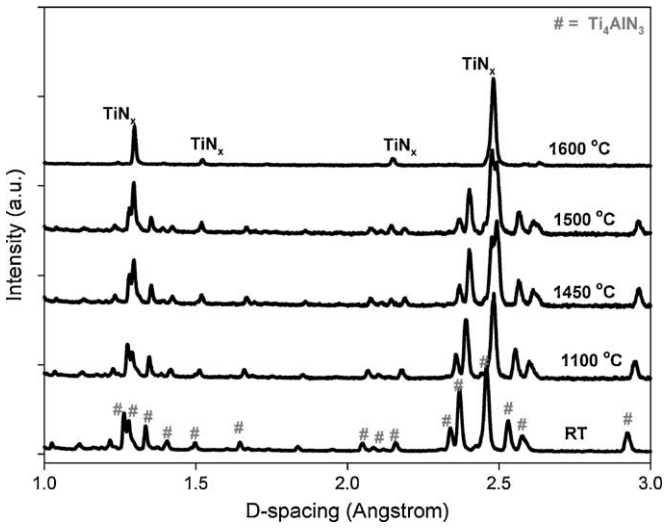

Fig. 1. Phase evolution during the vacuum decomposition of Ti_4AlN_3 at up to 1600 °C.

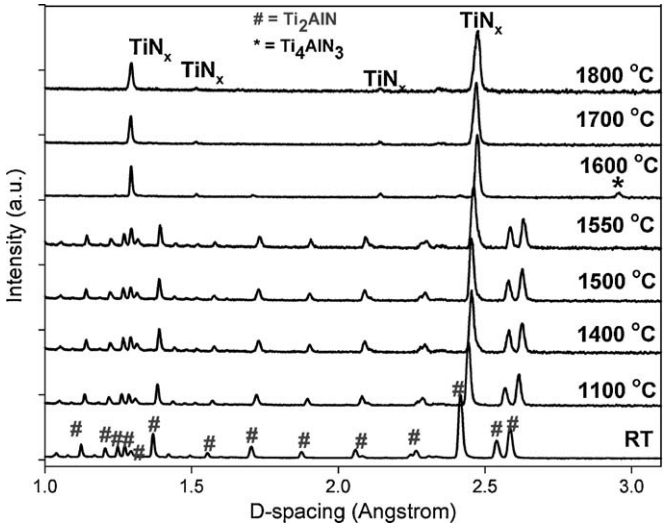

Fig. 2. Phase evolution during the vacuum decomposition of Ti_2AlN at up to 1800 °C.

3. Results and discussion

3.1. Thermal decomposition and phase transitions

The phase decompositions of Ti_2AlN and Ti_4AlN_3 at various temperatures as revealed by *in situ* neutron diffraction are shown in Figs. 1–3 and these are verified by the plots of synchrotron radiation diffraction patterns shown in Fig. 4. For Ti_4AlN_3, it began to decompose to TiN_x quite slowly at 1450 °C but became more rapid above 1500 °C (Fig. 1) and was almost completely decomposed after annealing at 1600 °C for less than 30 min. A total weight loss of ~11.6% and 5.9% was observed for ~2 h decomposition at 1600 and 1500 °C, respectively, which may

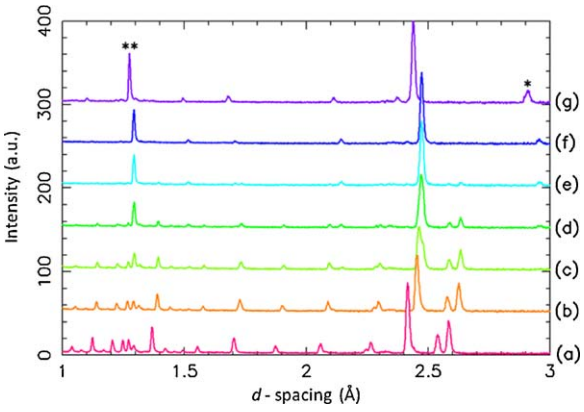

Fig. 3. Diffraction patterns of Ti_2AlN vacuum annealed at: (a) 20 °C; (b) 1400 °C; (c) 1600 °C/10 min; (d) 1600 °C/40 min; (e) 1600 °C/80 min; (f) 1600 °C/130 min; and (g): cooled to 20 °C. Note the formation of Ti_4AlN_3 at 1600 °C [legend: * = Ti_4AlN_3; ** = TiN].

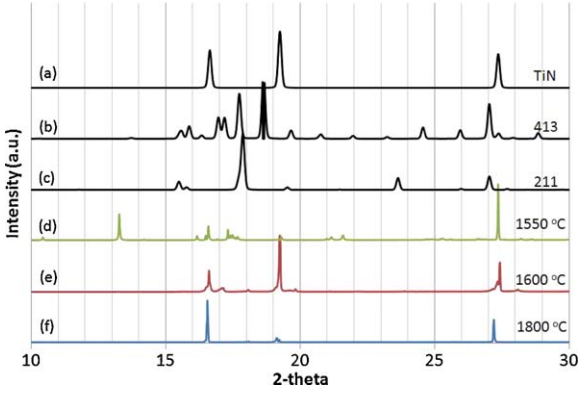

Fig. 4. Synchrotron radiation diffraction plots showing the diffraction patterns of (a) TiN, (b) Ti_4AlN_3, (c) Ti_2AlN, (d) Ti_2AlN vacuum-annealed at 1550 °C, (e) Ti_4AlN_3 vacuum-annealed at 1600 °C, and (f) Ti_2AlN vacuum-annealed at 1800 °C. Note that the plots for (a)–(c) are based on theoretical calculations.

be attributed mainly to the release of gaseous Al by sublimation during the decomposition process. This amount of weight loss is consistent with the fact that there is about 10.4 wt% of Al in Ti_4AlN_3 and these results concur with our previous work on ternary carbides.[9–12] It is worth mentioning that a lower order Ti_2AlN was not observed during the decomposition of Ti_4AlN_3 which suggests that a decomposition process via an intermediate 211 phase is thermodynamically impossible, i.e.,

$$Ti_4AlN_3 \neq Ti_2AlN + 2TiN \quad (4)$$

Instead, Ti_4AlN_3 decomposes directly to form $TiN_{0.75}$ via sublimation or de-intercalation of Al from its crystal layer structure, i.e.,

$$Ti_4AlN_3 \rightarrow 4TiN_{0.75} + Al_{(g)} \quad (5)$$

The Rietveld software Fullprof was used to analyse the neutron diffraction patterns for Ti_2AlN. The goodness-of-fit (GOF) ranged from 1.2 to 1.3 and satisfactory residual values of refinements were obtained for R_{wp} and R_B. Typical plots of Rietveld profile fit are shown in Fig. 5 for Ti_2AlN before and after vacuum decomposition. The distinct sample decomposition as a result of vacuum annealing at elevated temperature is evident.

The *in situ* decomposition of Ti_2AlN was observed to behave quite differently from that of Ti_4AlN_3. In spite of having a higher content of TiN as impurity, Ti_2AlN appeared to be much more stable against decomposition than Ti_4AlN_3. It began to decompose to TiN slowly after 1550 °C but became quite rapid at 1600 °C (Fig. 2). It was almost completely decomposed after annealing at 1700 °C for just over 2 h and at 1800 °C for about 20 min. A total weight loss of more than 20.0% was observed for decomposition at 1600 °C and above. Below 1600 °C, the weight loss was 5.0% and 0.95% at 1550 °C and 1500 °C, respectively. Noting that there is about 19.7 wt% of Al in Ti_2AlN, we deduce that the weight loss in decomposed Ti_2AlN is entirely due to sublimation of aluminium when its vapour pressure rises above the ambient pressure of the furnace. This is not surprising when we consider that the vapour pressure of aluminium metal rises rapidly from $\sim 7 \times 10^{-3}$ Torr at 1200 °C to ~0.5 Torr at 1500 °C. By contrast the vapour pressure for titanium metal is more than three orders of magnitude lower in this temperature range.[28] Thus, at temperatures higher than 1500 °C, we might expect Al to become quite volatile and sublime continuously in a dynamic environment of high vacuum, leading to severe decomposition of Ti_2AlN with the concomitant formation of non-stoichiometric TiN_x, i.e.,

$$Ti_2AlN_{(s)} \xrightarrow{T \geq 1500^\circ C} 2TiN_{0.5} + Al_{(g)} \quad (6)$$

However, the possibility of an additional but very small amount of Ti metal sublimation from the weak metallic Ti–C bonds cannot be ruled out because the vapour pressure of Ti is almost 10^{-2} Torr at 1700 °C. This conclusion was strongly supported by visual inspection of samples and furnace inserts after decomposition, where aluminium and possibly titanium coatings covered most surfaces.

A closer look at Fig. 2 shows that a new phase Ti_4AlN_3 formed when Ti_2AlN was vacuum-annealed at 1600 °C and its abundance increased with time and persisted when cooled down to room temperature (Fig. 3). This process of 211 → 413 transformation has also been reported by Hu et al.[29,30] for the decomposition of Ta_2AlC into Ta_4AlC_3 and Nb_2AlC to Nb_4AlC_3 in argon at high temperature, probably *via* the intercalation of the formed binary carbide into the 211 structure. However, it disappeared when the temperature was increased to 1700 °C and above.

We propose that the formation of Ti_4AlN_3 during vacuum annealing of Ti_2AlN at 1600 °C occurs *via* the intercalation of TiN in Ti_2AlN as follows:

$$Ti_2AlN_{(s)} + 2TiN_{(s)} \xrightarrow{1600^\circ C} Ti_4AlN_3 \quad (7)$$

At temperatures above 1600 °C, Ti_4AlN_3 becomes unstable and decomposes into $TiN_{0.75}$ *via* the sublimation of highly volatile Al (see Eq. (5)).

As previously mentioned, the weight losses of up to 11.6% and over 20% in decomposed Ti_4AlN_3 and Ti_2AlN, respectively, can be attributed to the release of gaseous Al (and possibly Ti) by sublimation during the decomposition process because the

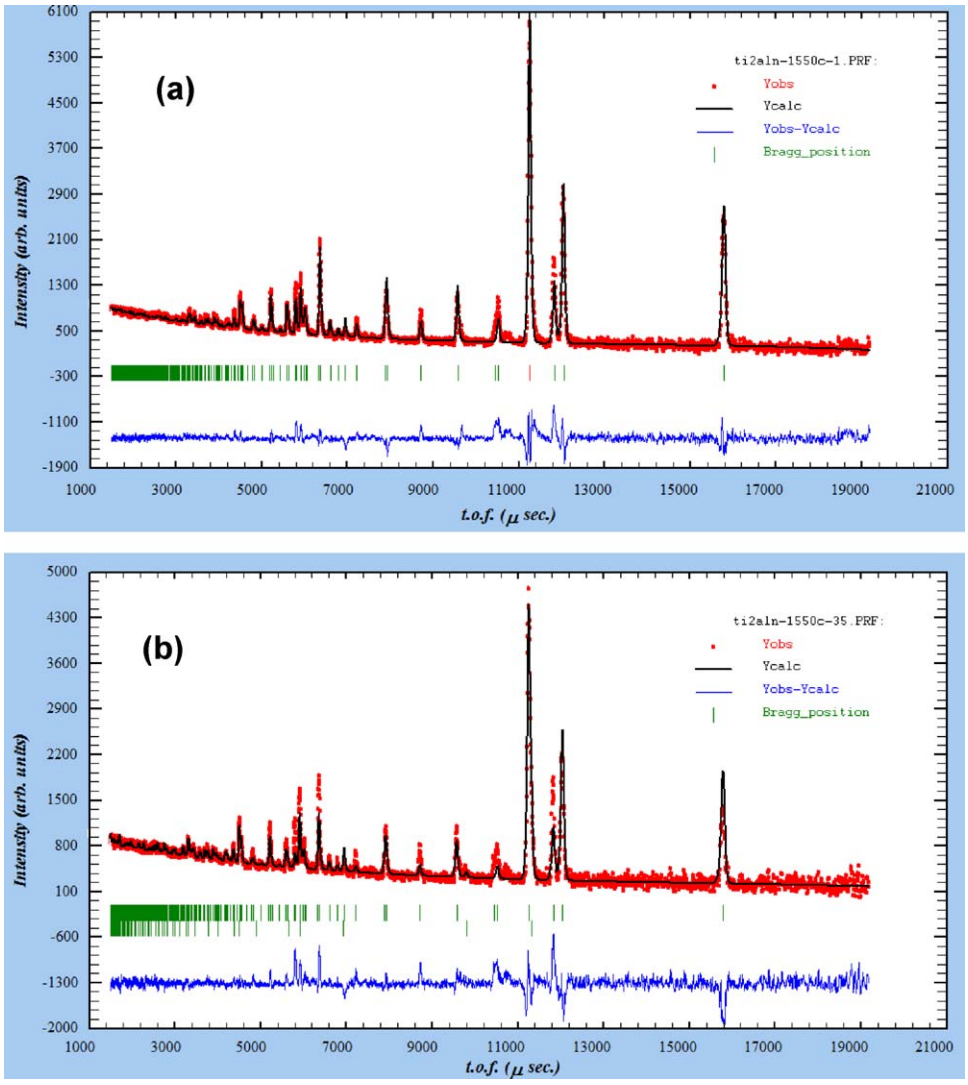

Fig. 5. The Rietveld profile fit of diffraction data of Ti_2AlN collected (a) before decomposition at 20 °C {GOF = 1.2; R_{wp} = 34.8; R_{exp} = 31.4} and (b) after vacuum annealing at 1550 °C {GOF = 1.2; R_{wp} = 47.9; R_{exp} = 43.7}. Measured patterns indicated by crosses, calculated pattern indicated by solid line. Intensity differences between the two patterns are shown along the bottom of the plot. Vertical bars represent the allowable peak positions for the phases. (Top: Ti_2AlN ICSD #52641; bottom: TiN_x ICSD #658338).

vapour pressures of both Al and Ti exceed the ambient pressure of the furnace (i.e., $\leq 5 \times 10^{-5}$ Torr) at ≥1500 °C.[28] Since the vapour pressure of a substance increases non-linearly with temperature according to the Clausius–Clapeyron relation,[31] the volatility of Al and Ti will increase with any incremental increase in temperature. Fig. 6 shows the vapour pressures of various elements at elevated temperature, and at a vapour pressure of 5×10^{-2} Torr in the vacuum furnace, both Al and Ti become volatile as the temperature approaches 1200° and 1700 °C, respectively. Thus, at the temperature of well over 1500 °C used in this study, both Al and a small amount of Ti should become volatile and sublime readily and continuously in a dynamic environment of high vacuum. When the vapour pressure becomes sufficient to overcome ambient pressure in the vacuum furnace, bubbles will form inside the bulk of the substance which eventually appear as voids on the surface of decomposed MAX phase.[9–12] The evidence of voids formation can be clearly discerned from the porous or "crater-like" surface damage of decomposed Ti_2AlN and Ti_4AlN_3 as shown in the optical photos of Fig. 7 and verified by the scanning electron micrographs in Fig. 8. A closer look of Fig. 6 may further explain why Ti_3SiC_2 is more resistant to decomposition than Ti_3AlC_2 or Ti_4AlN_3 because Si has a lower vapour pressure than Al. Thus, the use of vapour pressure of elements shown in Fig. 6 can be used to predict the susceptibility of MAX phases to thermal decomposition.

The variations of unit cell edges with temperature of all the phases and the corresponding coefficients of thermal expansion coefficient (CTE) are shown in Table 1. As would be expected, all the lattice parameters increased with increasing temperature by virtue of thermal expansion. However, the unit cell edges remained fairly constant with time up to 440 min at a particular isothermal annealing temperature. In addition, the calculated values of linear thermal expansion coefficient for Ti_4AlN_3 and Ti_2AlN shown in Table 1 are comparable with literature results.[1] However, it should be noted that the CTE of TiN_x reported here

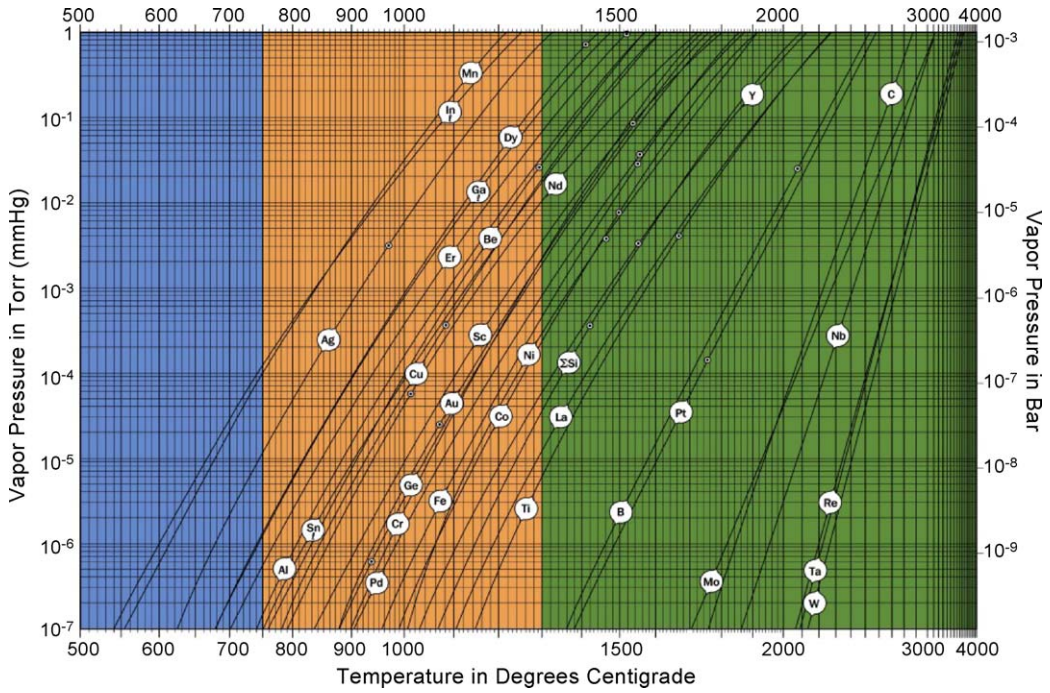

Fig. 6. Vapour pressure of selected elements at various temperatures.[28]

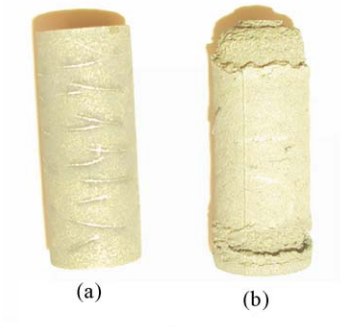

(i)

[(a) Before decomposition; (b) after decomposition at 1600°C for 440 min.]

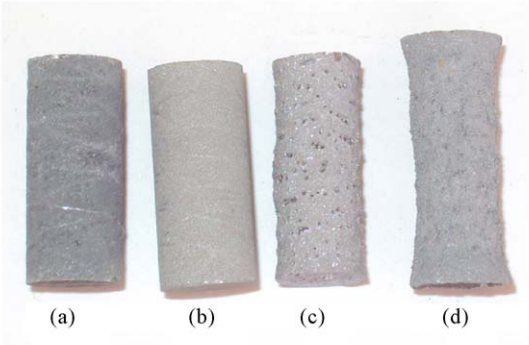

(ii)

[(a) Before decomposition; (b-d) after decomposition at 1500°C/120 min, 1700°C/40 min & 1800°C/20 min]

Fig. 7. Surface conditions of (i) Ti_4AlN_3 and (ii) Ti_2AlN before and after thermal decomposition during vacuum-annealing.

(i.e. $8.15 \times 10^{-6}\,K^{-1}$) is much lower than that of stoichiometric TiN which is about $9.35 \times 10^{-6}\,K^{-1}$).[1] This verifies the formation of non-stoichiometric TiN_x during vacuum-annealing of ternary nitrides at elevated temperature.

3.2. Isothermal phase decomposition and Avrami kinetics

Fig. 9 shows the phase composition, determined by measuring the area under the indicated Bragg reflections, during the isothermal decomposition of Ti_4AlN_3 at 1500 °C which was quite rapid initially but slowed down significantly after 30 min. More than 60% of Ti_4AlN_3 decomposed after vacuum annealing at 1500 °C for 400 min. In contrast, the decomposition for Ti_2AlN was much slower with only 20% decomposed after 300 min at 1550 °C (Fig. 10). This implies that Ti_2AlN has a significantly higher resistance to thermal decomposition

Table 1
Variations of unit cell edges as a function of temperature and the coefficient of linear thermal expansion (CTE) for Ti_2AlN, $Ti_4AlN_{2.9}$ and TiN_x.

Temperature (°C)	Ti_2AlN		$Ti_4AlN_{2.9}$		TiN_x
	a	*c*	*a*	*c*	*a*
25	2.984	13.579	2.994	23.402	4.244
1100	3.025	13.747	3.014	23.535	4.281
1400	3.036	13.794	3.020	23.573	4.292
1500	3.040	13.809	3.022	23.585	4.295
1550	3.042	13.817	3.023	23.591	4.297
1600	3.044	13.825	3.024	23.597	4.298
1700	–	–	–	–	4.302
1800	–	–	–	–	4.311
CTE (10^{-6}/°C)	12.746	11.493	6.340	5.302	8.153

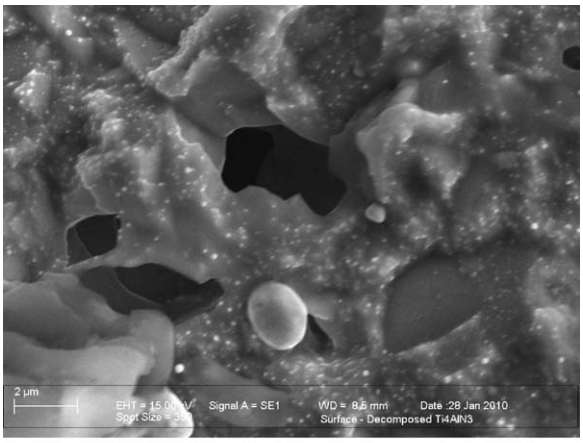

(a) Ti_4AlN_3

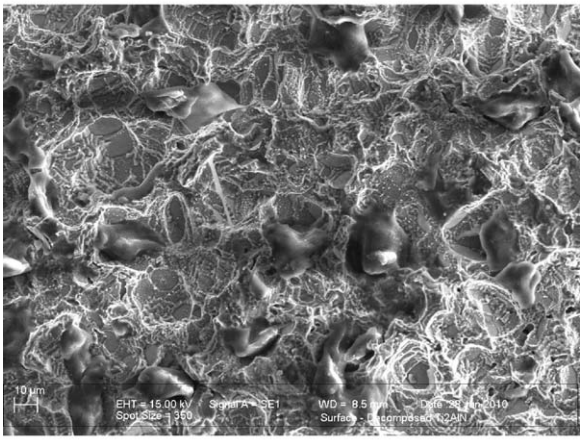

(b) Ti_2AlN

Fig. 8. Scanning electron micrographs showing the porous or "crater-like" surface microstructure of (a) Ti_4AlN_3 and (b) Ti_2AlN after thermal decomposition in vacuum at elevated temperature.

than Ti_4AlN_3. A possible reason for the high susceptibility of Ti_4AlN_3 to decomposition is either the existence of a lower order 211 phase or the much weaker Al-Ti bonding in this more complex layered compound where Al lies in every fifth layer.[1,3] In contrast, in the 211 compound the Al atoms are located in every third layer, resulting in shorter but stronger Al–Ti bonds which provides more resistance to decomposition via out-diffusion of Al from the bulk to the surface.

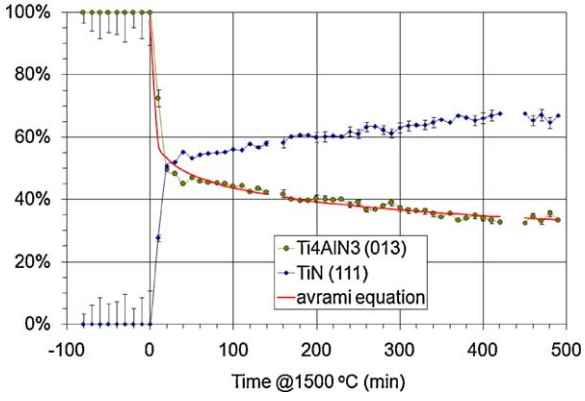

Fig. 9. Time-dependent phase abundance and Avrami fit of isothermal decomposition of Ti_4AlN_3 at 1500 °C.

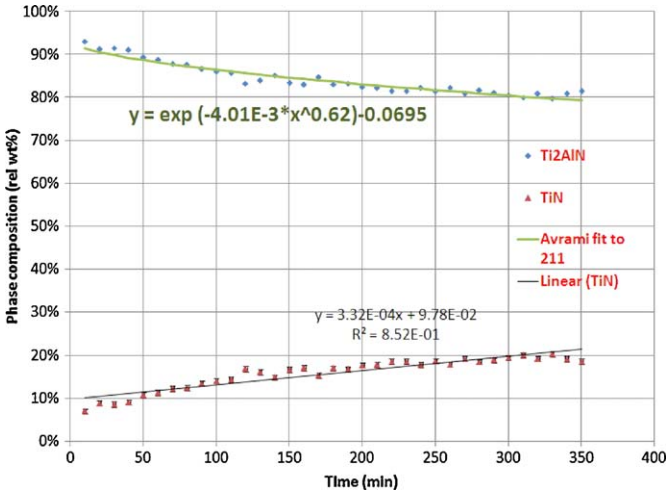

Fig. 10. Time-dependent phase abundance and Avrami fit of isothermal decomposition of Ti_2AlN at 1550 °C.

Table 2
Comparison of the Avrami decomposition kinetics in MAX 211 and 413 phases.

MAX phase	Avrami exponent (n)	Avrami constant (k) mol% $(min)^{-n}$
Ti_4AlN_3	0.18	0.37
Ti_2AlN	0.62	0.004

During the isothermal decomposition of 211 and 413 phases at 1550 and 1500 °C, the Avrami kinetics of decomposition was modelled using Eq. (3) and the Avrami constants were evaluated. The Avrami fit of the isothermal decomposition of Ti_4AlN_3 and Ti_2AlN is shown in Figs. 9 and 10, respectively. The calculated Avrami exponent (n) and Avrami constant (k) for the two MAX phases are summarised in Table 2. In general, when the value of n is large (e.g., 3 or 4), a 3-dimensional nucleation and growth process is involved.[32] High values of n can also occur when nucleation occurs on specific sites such as grain boundaries or impurities which rapidly saturate soon after the transformation begins. Initially, nucleation may be random and growth unhindered leading to high values for n. Once the nucleation sites are consumed the transformation will slow down or cease. Furthermore, if the distribution of nucleation sites is non-random then the growth may be restricted to 1 or 2-dimensions. Site saturation may lead to n values of 1, 2 or 3 for surface, edge and point sites, respectively.[21] Since the values of n obtained in this study for both 211 and 413 phases are less than 1.0, this implies that the decomposition process is driven by highly restricted out-diffusion of aluminium from the bulk to the surface of the sample and into the vacuum.

4. Conclusions

The high-temperature thermal stability of Ti_2AlN and Ti_4AlN_3 in a dynamic environment of high-vacuum has been studied using *in situ* neutron diffraction. Both 211 and 413 phases were susceptible to decomposition above 1400 °C

through sublimation of Al and possibly a small amount of Ti, resulting in a layer of TiN_x ($0.5 \leq x \leq 0.75$) being formed on the surface of the sample. The kinetics of isothermal phase decomposition was modelled using the Avrami equation and the Avrami constants n for the isothermal decompositions of Ti_2AlN and Ti_4AlN_3 indicate that in both cases the decomposition is a highly restricted diffusion process, presumably of aluminium from the bulk of the sample to its surface (from where it enters the vacuum of the furnace).

Acknowledgements

This work formed part of a much broader project on the thermal stability of ternary carbides which is funded by an ARC Discovery-Project grant (DP0664586) and an ARC Linkage-International grant (LX0774743) for one of us (I.M.L.). Neutron beamtime at ISIS (RB920121) was provided by the Science and Technology Facilities Council together with financial support from an AMRFP and LIEF grants (LE0882725). The collection of synchrotron diffraction data at the Photon Factory was funded by the Australian Synchrotron (AS101/ANBF2052).

References

1. Barsoum MW. The $M_{N+1}AX_N$ phases: a new class of solids: thermodynamically stable nanolaminates. *Prog Solid State Chem* 2000;**28**:201–81.
2. Zhang BH, Bao YW, Zhou YC. Current status in layered ternary carbide Ti_3SiC_2, a review. *J Mater Sci Technol* 2009;**25**:1–38.
3. Barsoum MW, El-Raghy T. The MAX phases: unique new carbide and nitride materials. *Am Sci* 2001;**89**:334–43.
4. Low IM. Vickers contact damage of micro-layered Ti_3SiC_2. *J Eur Ceram Soc* 1998;**18**:709–13.
5. Low IM, Lee SK, Barsoum MW, Lawn BR. Contact Hertzian response of Ti_3SiC_2 ceramics. *J Am Ceram Soc* 1998;**81**:225–8.
6. Low IM, Oo Z, Prince KE. Effect of vacuum annealing on the phase stability of Ti_3SiC_2. *J Am Ceram Soc* 2007;**90**:2610–4.
7. Low IM. Depth-profiling of phase composition in a novel Ti_3SiC_2–TiC system with graded interfaces. *Mater Lett* 2004;**58**:927–32.
8. Oo Z, Low IM, O'Connor BH. Dynamic study of the thermal stability of impure Ti_3SiC_2 in argon and air by neutron diffraction. *Physica B* 2006;**385–386**:499–501.
9. Pang WK, Low IM, Sun ZM. In-situ high-temperature diffraction study of thermal dissociation of Ti_3AlC_2 in vacuum. J Am Ceram Soc; in press.
10. Pang WK, Low IM, O'Connor BH, Studer AJ, Peterson VK, Sun ZM, et al. Comparison of thermal stability in MAX 211 and 312 phases. J Phys: Conf Ser; in press.
11. Pang WK, Low IM. Diffraction study of thermal dissociation in the ternary Ti–Al–C system. *J Aust Ceram Soc* 2009;**45**:39–43.
12. Pang WK, Low IM, O'Connor BH, Studer AJ, Peterson VK, Sun ZM, et al. Effect of vacuum annealing on the thermal stability of Ti_3SiC_2/TiC/$TiSi_2$ composites. *J Aust Ceram Soc* 2009;**45**:272–7.
13. Chen JX, Zhou YC, Zhang HB, Wan DT, Liu MY. Thermal stability of Ti_3AlC_2/Al_2O_3 composites in high vacuum. *Mater Chem Phys* 2007;**104**:109–12.
14. Wang XH, Zhou YC. Stability and selective oxidation of aluminium in nano-laminate Ti_3AlC_2 upon heating in argon. *Chem Mater* 2003;**15**:3716–20.
15. Barsoum MW, El-Raghy T. Synthesis and characterization of remarkable ceramic: Ti_3SiC_2. *J Am Ceram Soc* 1996;**79**:1953–6.
16. Radakrishnan R, Williams JJ, Akinc M. Synthesis and high-temperature stability of Ti_3SiC_2. *J Alloys Compd* 1999;**285**:85–8.
17. Emmerlich J, Music D, Eklund P, Wilhelmsson O, Jansson U, Schneider JM, et al. Thermal stability of Ti_3SiC_2 thin films. *Acta Mater* 2007;**55**:1479–88.
18. Zhang H, Zhou Y, Bao Y, Li M. Titanium silicon carbide pest induced by nitridation. *J Am Ceram Soc* 2008;**91**:494–9.
19. Feng A, Orling T, Munir ZA. Field-activated pressure-assisted combustion synthesis of polycrystalline Ti_3SiC_2. *J Mater Res* 1999;**14**:925–39.
20. Gao NF, Miyamoto Y, Zhang D. On physical and thermochemical properties of high-purity Ti_3SiC_2. *Mater Lett* 2002;**55**:61–6.
21. Tzenov N, Barsoum MW, El-Raghy T. Influence of small amounts of Fe and V on the synthesis and stability of Ti_3SiC_2. *J Eur Ceram Soc* 2000;**20**:801–6.
22. Lin ZJ, Zhuo MJ, Li MS, Wang JY, Zhou YC. Synthesis and microstructure of layered-ternary Ti_2AlN ceramic. *Scripta Mater* 2007;**56**:1115–8.
23. Rawn CJ, Barsoum MW, El-Raghy T, Procipio A, Hoffmann CM, Hubbard CR. Structure of Ti_4AlN_3: a layered $M_{n+1}AX_n$ nitride. *Mater Res Bull* 2000;**35**:1785–96.
24. Hull S, Smith RI, David W, Hannon A, Mayers J, Cywinski R. The POLARIS powder diffractometer at ISIS. *Physica B* 1992;**180-181**:1000–2.
25. Rietveld HM. A profile refinement method for nuclear and magnetic structures. *J Appl Crystallogr* 1969;**2**:65–71.
26. Cahn JW. Transformation kinetics during continuous cooling. *Acta Metall* 1956;**4**:572–5.
27. O'Connor BH, van Riessen A, Carter J, Burton GR, Cookson DJ, Garrett RF. Characterization of ceramic materials with BIGDIFF: a synchrotron radiation Debye–Scherrer powder diffractometer. *J Am Ceram Soc* 1997;**80**:1373–81.
28. www.veeco.com/library/Learning_Center/Growth_Information/Vapor_Pressure_Data_For_Selected_Elements/index.aspx.
29. Hu C, Zhang J, Bao Y, Wang JY, Li M, Zhou YC. In-situ reaction synthesis and decomposition of Ta_2AlC. *Z Metallkd* 2008;**99**:8–13.
30. Hu C, Li F, Zhang J, Wang JM, Wang JY, Zhou YC, et al. A new compound belonging to the MAX phases. *Scripta Mater* 2007;**57**:893–6.
31. Callen HB. *Thermodynamics and an introduction to thermostatistics*. London: Wiley; 1985.
32. Jena AK, Chaturvedi MC. *Phase transformations in materials*. New York: Prentice Hall; 1991.